Chemical Science

ROYAL SOCIETY OF CHEMISTRY

EDGE ARTICLE

View Article Online
View Journal | View Issue

Cite this: *Chem. Sci.*, 2024, **15**, 15321

All publication charges for this article have been paid for by the Royal Society of Chemistry

Received 12th May 2024
Accepted 26th August 2024

DOI: 10.1039/d4sc03106g

rsc.li/chemical-science

Integrated "all-in-one" strategy to construct highly efficient Pd catalyst for CO_2 transformation†

Lingfang Kong,‡[a] Zekun Tao,‡[a] Yunjia Li,[a] Huiwen Gong,[a] Yun Bai,[a] Longbin Li,[a] Xianjin Zhang,[b] Zhonggao Zhou *[a] and Yiwang Chen *[a]

The synthesis of high-value chemicals featuring C–C and/or C–heteroatom bonds *via* CO_2 is critically important, yet efficiently converting thermodynamically stable and kinetically inert linear CO_2 and propargylic amine to the heterocyclic compound 2-oxazolidinone with an integrated catalytic system continues to pose a considerable challenge. Herein, we have designed an "all-in-one" (AIO) palladium (Pd) catalyst (Cat**1**), distinguished by its co-coordination with acetylglucose (AcGlu) and bis(benzimidazolium) units at the Pd center, which promotes the cyclization of CO_2 and propargylic amine achieving a highest turnover frequency (TOF) of up to 3456 h^{-1}. Moreover, Cat**1** demonstrates excellent stability across various temperatures, with its catalytic activity remaining unchanged even after 10 cycles. The catalyst Cat**1** simultaneously activates propargylic amine and CO_2, facilitating the formation of N-heterocyclic carbene (NHC)-CO_2 adducts and AcGlu-CO_2 philes from CO_2 in simulated flue gas, a key factor in reaching unprecedented TOF values. The catalytic mechanism was elucidated through *quasi-in-situ* NMR and ^{13}C-isotope labeling experiments. Notably, this is the first instance of an AIO Pd catalyst that enables the simultaneous capture, activation, and catalytic conversion of *in-situ* activated CO_2 along with propargylic amine. The design strategy of this AIO catalyst introduces a novel approach to overcoming the challenges in the efficient conversion of inert CO_2.

Introduction

The substantial consumption of fossil fuels accelerates carbon dioxide (CO_2) emissions and causes a severe environmental crisis, prompting significant efforts to mitigate, capture, and utilize excess CO_2.[1–7] Among various conversion approaches, the preparation of 2-oxazolidinone through CO_2 conversion plays a critical role as a heterocyclic compound in the realms of chemistry, medicine, and polymer science.[8–10] Recent advances in ionic liquids (ILs), N-heterocyclic carbenes (NHCs), N-heterocyclic olefins (NHOs), metal–organic frameworks (MOFs), organic acids and bases, and metal catalysts have facilitated the synthesis of 2-oxazolidinones (Fig. 1a, such as PNU-85055, Spirooxazolidinone C, *etc.*) from propargylic amines and CO_2.[11–13] As present in Fig. 1b, for example, Inagaki *et al.* reported that the gold catalyst [Au(dpb^F)]X, featuring a Z-type ligand, exhibited a turnover frequency (TOF) value of 5.3

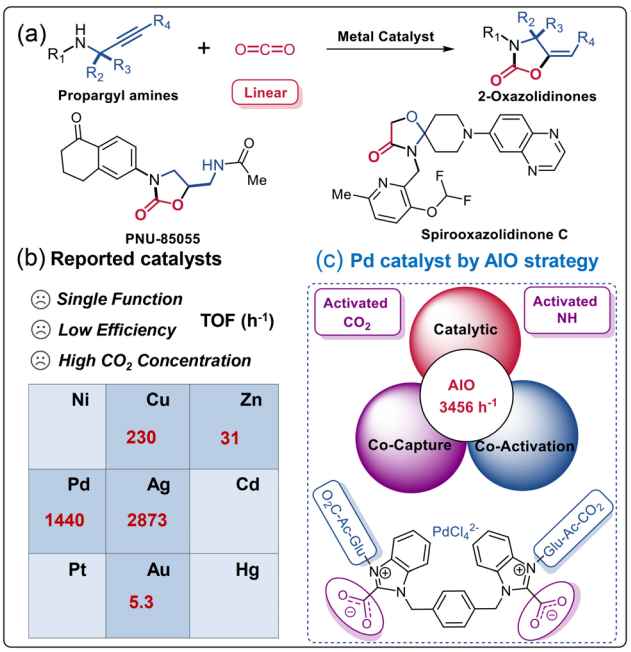

Fig. 1 (a) The metal-catalyzed cyclization of propargylic amines and CO_2. (b) The reported metal catalysts with different TOFs, see attached Table S1† for more detailed parameters. (c) Pd catalyst construct by integrated AIO strategy herein.

[a]*College of Chemistry and Chemical Engineering/Analysis and Testing Center/Key Laboratory of Jiangxi University for Functional Materials Chemistry, Gannan Normal University, Ganzhou 341000, P. R. China. E-mail: zhgzhou@foxmail.com; ywchen@ncu.edu.cn*

[b]*Institute of Chemistry Education, Fujian Institute of Education, Fuzhou 350025, P. R. China*

† Electronic supplementary information (ESI) available. See DOI: https://doi.org/10.1039/d4sc03106g

‡ L. Kong and Z. Tao contributed equally to this work.

h^{-1}, possibly attributed to the σ-acceptance of the borane atom.[14] Zhao and co-authors discovered that the noble-metal-free lantern-like, eco-friendly [Zn_{116}] nanocages catalyst achieved a TOF value of 31 h^{-1},[15] and a mixed valence copper-based cationic MOFs catalyst achieved an impressive TOF value of 230 h^{-1}.[16] Our group also demonstrated that Pd catalyst AcGlu-MeIm-$PdCl_4$ can achieve a TOF value of 1440 h^{-1}.[17] Zhu *et al.* highlighted the exceptional catalytic activity of a low-nuclear customized Ag_4 NC, with turnover number (TON) and TOF values reaching 5746.2 and 2873.1 h^{-1} respectively.[11] This catalytic system demonstrated concurrent capture, activation, and catalytic conversion of *in-situ* activated CO_2 alongside propargylic amine, indicating its efficacy in facilitating these reactions. However, due to the kinetic inertness and thermodynamic stability of linear CO_2, significant challenges persist in its efficient activation and conversion. Clearly, the activation of inert CO_2 is a crucial step in reducing the energy required for subsequent reactions involving CO_2 as a reactant. From a practical perspective, the direct transformation of low-concentration CO_2 (such as simulated flue gas, CO_2 concentration 15–30%) into desirable products should be an ideal alternative as it can avoid the high energy consumption from the separation and concentration of anthropogenic CO_2.[18,19]

Numerous Lewis base (LB)-CO_2 adducts have been employed to activate CO_2 and developed as organocatalysts, including organic phosphine, organic amine, alkoxide-functionalized imidazolium betaines, free NHOs, and phosphorus-ylide systems.[20–23] The strong σ-donor character of free NHC has also been utilized for CO_2 capture, and the resulting NHC-carboxylates or NHC-CO_2 adducts have been applied as effective organocatalysts and activated CO_2 sources.[24–27] However, the *in-situ* capture of CO_2 as LB-CO_2 adducts and its subsequent transformation *via* metal catalysis remain challenging, with limited studies.[17,28] Consequently, the pursuit of developing highly efficient integrated metal catalysts that can transform CO_2, specifically from *in-situ* formed LB-CO_2, into value-added chemicals without requiring extra additives, stands as a paramount goal for the scientific community. The "all-in-one" (AIO) strategy for constructing efficient catalysts is an emerging approach that combines the unique properties of traditional metallic, organic, and inorganic analogs due to its hybrid nature.[29–31] ILs possess many excellent characteristics, such as the ability to dissolve acidic gases, high thermal stability, and low vapor pressure, which meet the requirements in CO_2 capture.[32–36] Metal-containing imidazolium ILs have been recognized as potential NHC ligand, NHC-metal catalyst precursor, and reaction reagents for various transformations.[37–39] However, the *in-situ* formation of NHC-CO_2 adducts from metal-containing imidazolium ILs for catalytic CO_2 conversion shows great promise, yet has not been realized.

Sugar acetates (SAs) featuring acetyl (Ac) units present a unique strategy for the capturing and activating of CO_2 through CO_2-philes.[40–44] Tsivintzelis *et al.* found that composite membranes made from cellulose acetate, which exhibited high CO_2 affinity, are utilized for separating CO_2 from natural gas or in CO_2/N_2 mixed gas.[45] The interactions between CO_2 and a combination of α-D-glucose pentaacetate (GPA) and [Bmim][BF_4] ILs (−25.3 kJ mol^{-1}) are notably stronger than those in GPA···CO_2 (−10.7 kJ mol^{-1}) and [Bmim][BF_4]···CO_2 (−17.8 kJ mol^{-1}) when examined independently. These interactions offer additional benefits including non-toxicity and cost-effectiveness.[40] In addition, integrating SAs into ILs significantly enhances the interactions between metals and SAs, thereby greatly improving their effectiveness in metal-catalyzed reactions with increased catalytic activity.[17,46–50] It is thus plausible to propose that SAs and ILs can jointly activate CO_2 and stabilize metal catalytic species during the catalysis process. The utilization of Pd catalysts for synthesizing important, biologically active heterocyclic compounds has attracted considerable research attention.[51–53] Despite substantial efforts to develop various Pd catalysts for CO_2 transformation,[17] challenges such as low turnover frequency (TOF), catalytic efficiency, high CO_2 concentration, and high catalyst loading persist. Therefore, developing a robust, high-performance AIO Pd catalyst for the capture, activation, and catalytic transformation (CACT) of CO_2 remains a formidable and intriguing research area.

Herein, we designed a series of metal-containing bis(benzimidazolium) ILs (Cat**1-5**), specifically engineered for the CACT of CO_2 and propargylic amines (Fig. 1a, R_4 = H). These chloropalladate-containing ILs were facilitated synthesized *via* a biphasic ion exchange reaction between the respective bis(-benzimidazolium) bromide salts (Im-Br**1-4**) and Na_2PdCl_4. We further evaluated the catalytic performance of Cat**1-5** in the CACT of CO_2 and propargylic amines. The integrated Cat**1** catalytic system, containing AcGlu and bis(benzimidazolium) units, demonstrated a synergistic effect with Pd in the CACT of *in situ* activated-CO_2, forming NHC-CO_2 adducts and AcGlu-CO_2-philes. This stimulation activation of CO_2 and propargylic amine ensures reached a highest reported TOF value of 3456 h^{-1} (Fig. 1c). In addition, Cat**1** exhibits good stability across a range of temperatures, effectively integrating the advantages of homogeneous catalysis and catalyst recycling, and can be reused for at least 10 cycles without significant loss in catalytic performance. ^{1}H NMR experimentals confirmed that AcGlu and bis(benzimidazolium) co-coordinated Cat**1**, providing multiple LA-LB sites for the activation of CO_2, propargylic amine, and stabilization of Pd catalyst species. The catalytic mechanism was elucidated through *quasi-in-situ* NMR and ^{13}C-isotope-labeling experiments.

Results and discussion

Reasonable design, preparation, and characterization of Pd catalysts

At the outset of our study, acetylglucoside bis(benzimidazolium) tetrachloropalladate salts (Cat**1-3** and **5**) were synthesized in four steps from natural D-glucose. The final step involved a straightforward ion exchange of the corresponding bromide salts (Im-Br**1-3** and **5**) with Na_2PdCl_4 (Fig. 2a). For comparative purposes, a bis(benzimidazolium) tetrachloropalladate salt (Cat**4**) featuring an *n*-octyl (–$^nC_8H_{15}$) side chain was synthesized using a similar method. Cat**5** and Im-Br**5** were also obtained by

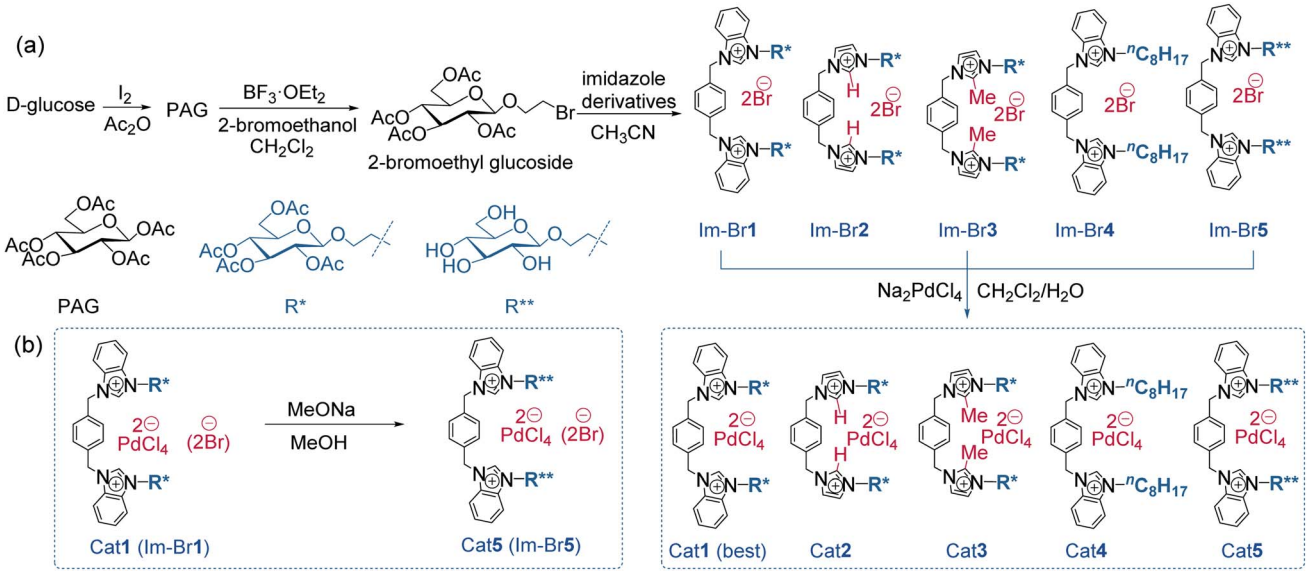

Fig. 2 (a) The synthetic routes of Pd catalysts Cat**1-5**. (b) The synthesis route of bromide salt Im-Brc**1** and Pd catalyst Cat**5**.

deprotecting the Ac groups from the corresponding Cat**1** and Im-Br**1** (Fig. 2b), primarily to investigate their roles in the catalytic process. Cat**1-5** can be synthesized with high purity and are readily available in large quantities with high yields. It is worth noting that the use of 2-bromoethyl glucoside is intended to alleviate steric hindrance between the anomeric equatorial carbon of the sugar and the axial C_2–H of the imidazolium ring by introducing an ethyl group to separate them.[49] This design also helps to minimize potential interactions between the imidazolium ring and sugar units in order to evaluate their role during the catalytic process.

All these compounds were thoroughly characterized using ^{1}H and ^{13}C nuclear magnetic resonance spectra (NMR, Fig. S1–S10†), Fourier-transform infrared spectra (FT-IR, Fig. S11–S15†), and liquid chromatography-high-resolution mass spectrometry (LC-HR/MS, Fig. S16–S25†). Furthermore, X-ray photoelectron spectroscopy (XPS, Fig. S26†) was employed to discern the distinct chemical coordination environments of Cat**1** and Cat**5**, with and without Ac protecting groups. Meanwhile, thermal stability of Cat**1-5** was also studied using thermogravimetric analysis (TGA, Fig. S27†). The NMR signals of Cat**1-5** closely resembled those of their corresponding bromide salts (Im-Br**1-5**), with the most notable peaks appearing in similar regions across spectra (Fig. S1–S10†). Specifically, the characteristic imidazolium C_2–H singlet peak in the bromide salts Im-Br**1-2** and **4-5** was observed at δ 9.80∼10.40 ppm, shifting to δ 9.3∼10.10 ppm in Cat**1-2** and **4-5** after ion exchange. The multiplets for C_{1-6}–H in glucoside of Im-Br**1-3** and **5**, ranging from δ 3.20–5.90 ppm, were comparable to those in Cat**1-3** and **5**, also shifting to δ 9.3∼10.10 ppm. ^{13}C NMR spectra revealed a significant peak for C_2–C in Im-Br**1-5** at δ 137.0∼145.4 ppm, slightly altered to δ 136.4∼145.4 ppm in Cat**1-5**. NMR results showed that the introduction of $PdCl_4^{2-}$ anion not only maintained the original structure of the parent compound, but also enhanced its interaction with AcGlu groups and benzimidazolium cation. FT-IR spectra indicated absorption peaks at approximately 1563 and 1630 cm^{-1}, attributed to the C=N and C=C stretch vibrations of the imidazolium unit in Cat**1-5**. Additional signals at about 1172, 1126, and 1035 cm^{-1} were consistent with C–H bending vibrations in the imidazolium rings of Cat**1-5** (Fig. S11–S15†). LC-HR/MS analysis in positive mode confirmed the presence of only imidazolium cations, with indistinguishable test signals for Cat**1-5** and Im-Br**1-5** (Fig. S16–S25†), corroborating our previously reported results.[17] The chemical environment of the key elements in the near-surface region of Cat**1** and Cat**5** was further characterized using XPS. Carbon was the predominant element, with the XPS spectrum of Cat**5** resolving into component parts corresponding to C–C (∼284.8 eV), C–N (∼286.7 eV), and C=O/O–C=O (∼289.2 eV).[31] Pd 3d XPS spectra for Cat**5** displayed peaks at 337.7 (Pd $3d_{5/2}$) and 343.2 eV (Pd $3d_{3/2}$), indicative of Pd in the +2 oxidation state and substantial electron donation from AcGlu and bis(benzimidazolium) units to the $PdCl_4^{2-}$ anions (Fig. S26†).[54] Notably, the Pd 3d XPS spectra of Cat**5** without Ac protecting groups also showed significant shifts (0.6–0.7 eV) in the binding energies of benzimidazolium heterocycles, suggesting increased electron delocalization after ion exchange. These experimental results confirmed the successful synthesis of the target products Im-Br**1-5** and Cat**1-5**. The TGA curves show that the decomposition temperatures of catalysts Cat**1-5** range from 186 °C to 225 °C (Fig. S27†), indicating their good thermal stability. Furthermore, Cat**1** was dissolved in dimethyl sulfoxide (DMSO-d_6) and maintained at various temperatures (−22 °C, 25∼30 °C, and 70 °C) for 10 h to assess its stability in solution. Remarkably, no significant changes were observed in its ^{1}H, ^{13}C NMR spectrum, and color across these different environments (Fig. S28†). These results suggest that Cat**1** is stable and does not undergo decomposition during the catalytic reaction.

Catalytic activity evaluation

Initially, the catalytic performance of Cat**1** was evaluated in the model reaction of *N*-(4-methoxybenzyl)propargylic amine (**6a**) and CO_2 [simulated flue gas, $V(CO_2):V(N_2) = 15:85$] at 70 °C with NaO^{t}Bu in different solvents (Fig. 3a). No reaction was observed in tetrahydrofuran (THF), and a 10% yield of the product 3-(4-methoxybenzyl)-5-methyleneoxazolidin-2-one (**7a**) was observed in acetonitrile (CH_3CN). However, good to excellent yields of **7a** (80–92%) were obtained in 1,4-dioxane (Diox), ethanol (EtOH), and methanol (MeOH). Remarkably, nearly 100% yields were achieved in *N*,*N*-dimethylformamide (DMF) and DMSO within 2.0 h. Further optimization of the reaction time revealed that DMSO was the superior solvent, yielding a higher TOF (89.6 h^{-1}) compared to DMF (25.6 h^{-1}). These results align with those previously reported by C. Nevado using $PdCl_2$(dppf),[55] and by D. Bourissou using a Pd SCS complex.[56] Additionally, the interaction energies of the DMSO-CO_2 complexes at the MP2 level indicate effective CO_2 activation,[44] facilitating faster reaction kinetics in DMSO. Subsequently, we optimized various bases in DMSO (Fig. 3b). In the presence of inorganic bases such as NaOH, NaOAc, $Na_3PO_4\cdot12H_2O$, and Na_2CO_3, substrate **6a** was completely consumed, yielding product **7a** in approximately 100% yields. KOH, K_2CO_3, and $NaHCO_3$ produced yields of 96%, 95%, and 10%, respectively. The weak organic base triethylamine (TEA) afforded only a 29% yield. In contrast, the strong organic bases 1,8-diazabicycloundec-7-ene (DBU) and NaO^{t}Bu favorably promoted the reaction, yielding 88% and approximately 100% yields, respectively.

As expected, no product was detected in the absence of a base. By optimizing the reaction time and catalyst dosage, we determined that the weak inorganic base NaOAc, which contains acetate anions (OAc^-, Fig. 3c), was the optimal choice, achieving a TOF of 100 h^{-1} with 100% yield, which could further increase to 672 h^{-1}. Rogers *et al.* observed that the introducing CO_2 into 1,3-dialkylimidazolium acetate ILs *via* bubbling facilitated the formation of corresponding NHC-CO_2 adducts.[57] Consequently, it is plausible that the activity of CO_2 manifested in the form of NHC-CO_2 adducts, arising from free NHC generated *in situ* following the reaction between benzimidazolium cations and NaOAc. Further assessment of various temperatures revealed a notable impact on the reaction process (Fig. 3d). At room temperature (RT, approximately 20–25 °C), only 28% yield of **7a** was obtained, with yields increasing to 30–68% as the temperature rose from RT to 70 °C. However, a significant reduction in yield to 54% occurred when the temperature was increased to 80 °C. These results indicate that high temperatures are not conducive to the reaction, primarily due to the decomposition of the *in-situ* formed NHC-CO_2 adducts and DMSO-CO_2 complexes at elevated temperatures.[17,27,28,58]

By comparing the catalytic activities of AIO Pd catalyst Cat**1-5** (Table 1, entries 1–5), we observed that Cat**1**, containing AcGlu and bis(benzimidazolium) units, exhibited superior performance with a TOF of 2400 h^{-1}, 100% yield, and TON of 400 (entry 1). Other catalysts, such as Cat**2**, Cat**3**, and Cat**4**, were less efficient, yielding 94%, 91%, and 52% respectively (entries 2–4). Cat**5** without Ac protecting groups, when used as a catalyst, yielded only 36% with a TOF of 864 h^{-1}. This comparison highlights the critical role of Ac units in enhancing catalytic performance. To elucidate the role of functional units in Cat**1**,

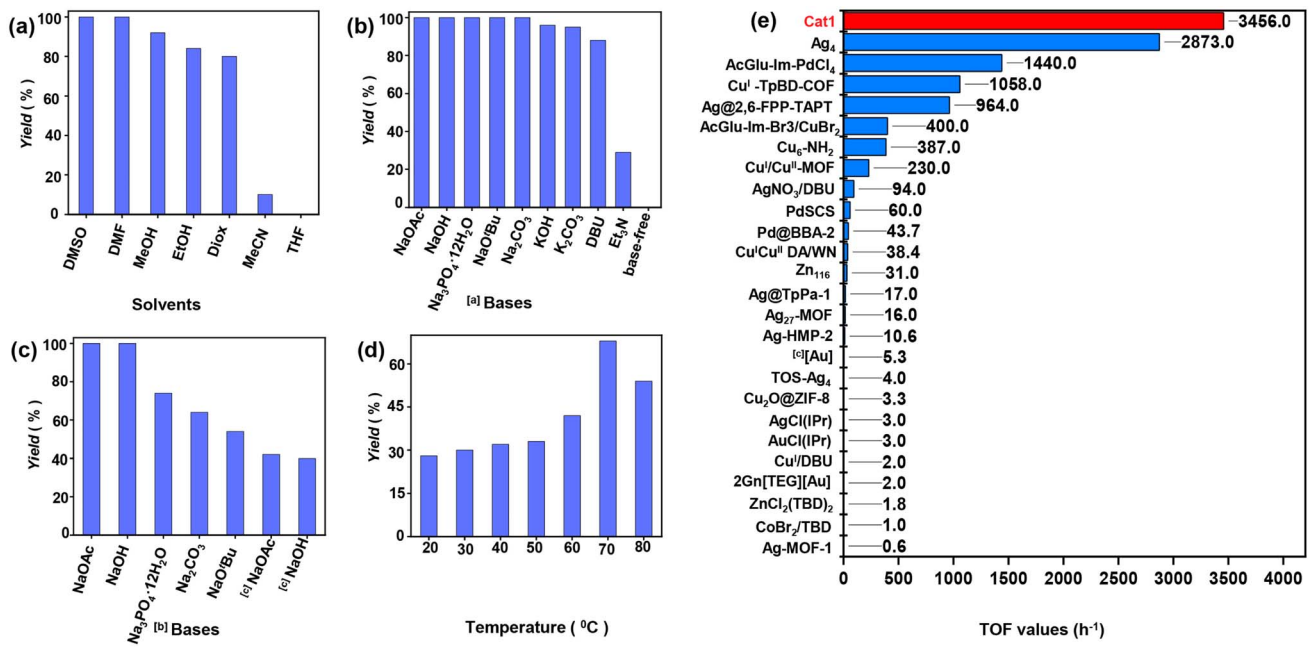

Fig. 3 Screening the reaction of **6a** with CO_2 (simulated flue gas, bubbling) under various conditions, Pd catalyst (0.5 mol%), base (0.15 mmol), solvent (2.0 mL), and stirred at 70 °C for 1.0 h, unless noted otherwise, yields were determined by ^{1}H NMR. The reactions were carried out with different solvents (a), bases (b and c), and (d) temperatures. [a] DMSO (2.0 mL). [b] 0.25 h. (e) Comparison with other reported catalysts. TOF was calculated using optimal conditions reported in the literature. Detailed reaction conditions are provided in Table S1.†

Table 1 Screening of the reaction conditions

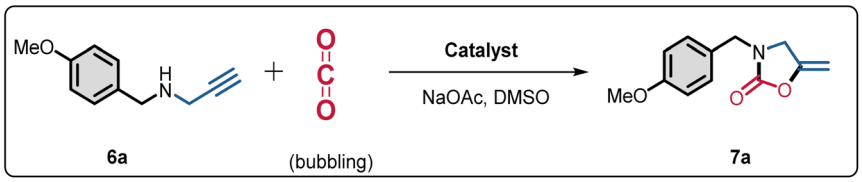

Entry[a]	Catalyst	Yields[b] [%]	TOF [h^{-1}]	TON
1	Cat**1**	100[c], 74[d]	2400[c], 3456[d]	400[c], 288[d]
2	Cat**2**	94[c]	2256	376
3	Cat**3**	91[c]	2184	364
4	Cat**4**	52[c]	1242	207
5	Cat**5**	36[c]	864	144
6	K_2PdCl_4	28	56	56
7	$Pd(OAc)_2$	44	88	88
8	$PdCl_2$	37	74	74
9	Im-Br**1**/K_2PdCl_4	70	140	140
10	Im-Br**1**/$Pd(OAc)_2$	64	128	128
11	Im-Br**1**/$PdCl_2$	71	142	142
12	PAG/K_2PdCl_4	56	112	112
13	Blank, Im-Br**1**	n.d.[e]	—	—

[a] The reactions were carried out with **6a** (0.1 mmol), Pd catalyst (0.5 mol%), CO_2 (simulated flue gas, bubbling), NaOAc (0.15 mmol), DMSO (1.0 mL) and stirred at 70 °C for 1.0 h, unless noted otherwise. [b] Determined by ^1H NMR. [c] Catalyst (0.25 mol%), CO_2 (1.0 atm, bubbling), 10 min. [d] Catalyst (0.25 mol%), CO_2 (simulated flue gas, bubbling), NaOAc (0.15 mmol), 5 min. [e] **7a** was not detected (n.d.).

various Pd catalyst systems were evaluated (entries 6–11). When commercial catalysts like K_2PdCl_4, $Pd(OAc)_2$, and $PdCl_2$ were used directly, they achieved only 28%, 44%, and 37%, respectively (entries 6–8). When combined with Im-Br**1**, these catalysts' activities significantly improved, resulting in 70%, 64%, and 71% yields (entries 9–11). Furthermore, the yield rose significantly to 56% (entry 12) when glucose pentaacetate (PAG) was used in conjunction with the pure K_2PdCl_4 catalyst, which had a yield of only 28% (entry 6). This suggests that both PAG and Im-Br**1** enhance the activity of palladium species. In the absence of any Pd catalyst (entry 13), and with only Im-Br**1** used, no product was detected. In addition, it was also observed that increasing the amount of NaOAc from 1.5 to 4.0 equivalents significantly boosted the yield to 74% and achieved the highest reported TOF (3456 h^{-1}) and TON (288, entry 1), underscoring the pivotal role of OAc^- herein. The TOF value of Cat**1** surpasses that of all other previously reported homogeneous and heterogeneous catalytic systems for the reaction of propargylic amines and dilute CO_2, as detailed in Fig. 3e and Table S1.†

During the optimization process, we observed significantly variation in the conversion of **6a** as reaction time and temperature increased. Consequently, a series of detailed kinetic experiments were thus performed to validate the impact of various on the conversion of **6a**. Derived simplified kinetic equations based on existing literature reports:[59,60]

$$\ln(1 - x) = -k_{obs}t + C \quad (1)$$

where k_{obs} is the rate constant, t is the reaction time (min), x is the **6a** conversion (%). The kinetics of the reaction were investigated using eqn (1), and the rate constants (k_{obs}) were determined by analyzing the slope of the linear relationship between $\ln(1 - x)$ and t. The resulting experimental data can be found in Fig. S29.† Notably, all conditions yielded correlation coefficients with squared values close to 1, indicating a strong indication that the reaction is a first-order process concerning **6a** concentration, catalyst dosage, and CO_2 flow rate.

With the optimal reaction conditions established, we further evaluated substrates with various substituents on the benzyl ring (Fig. 4). Both electron-withdrawing and electron-donating groups, regardless of their positions, were well tolerated, delivering the desired products **7a-h** yields ranging from 90% to 100%. This protocol proved efficient for 3-methoxy (**7b**), 2,6-difluoro (**7c**), 4-fluoro (**7d**), 4-bromo (**7e**), 4-chloro (**7f**), and 4-trifluoromethyl (**7g**) substituents. Propargylic amines with 3-butyl (**6i**) and 3-cyclohexylmethyl (**6j**) substituents were also efficiently converted into the corresponding 2-oxazolidinones (**7i** and **7j**) in excellent yields (up to approximately 100%). Notably, the reaction proceeded smoothly with propargylic amines bearing both electron-withdrawing and electron-donating groups.

The introduction of a methyl substituent at the benzylic position, increasing steric hindrance, notably affected the yields, producing desired products (**7k** and **7l**) in moderate yields. Extending the reaction time to 2.0 h also facilitated the efficient conversion of propargylic amines **6k** and **6l** into the corresponding products **7k** and **7l** in excellent yields (92% and 94%). Unfortunately, when R_4 was a Me- group, the substrates **6n–6p** exhibited relatively low reactivity, illustrating the

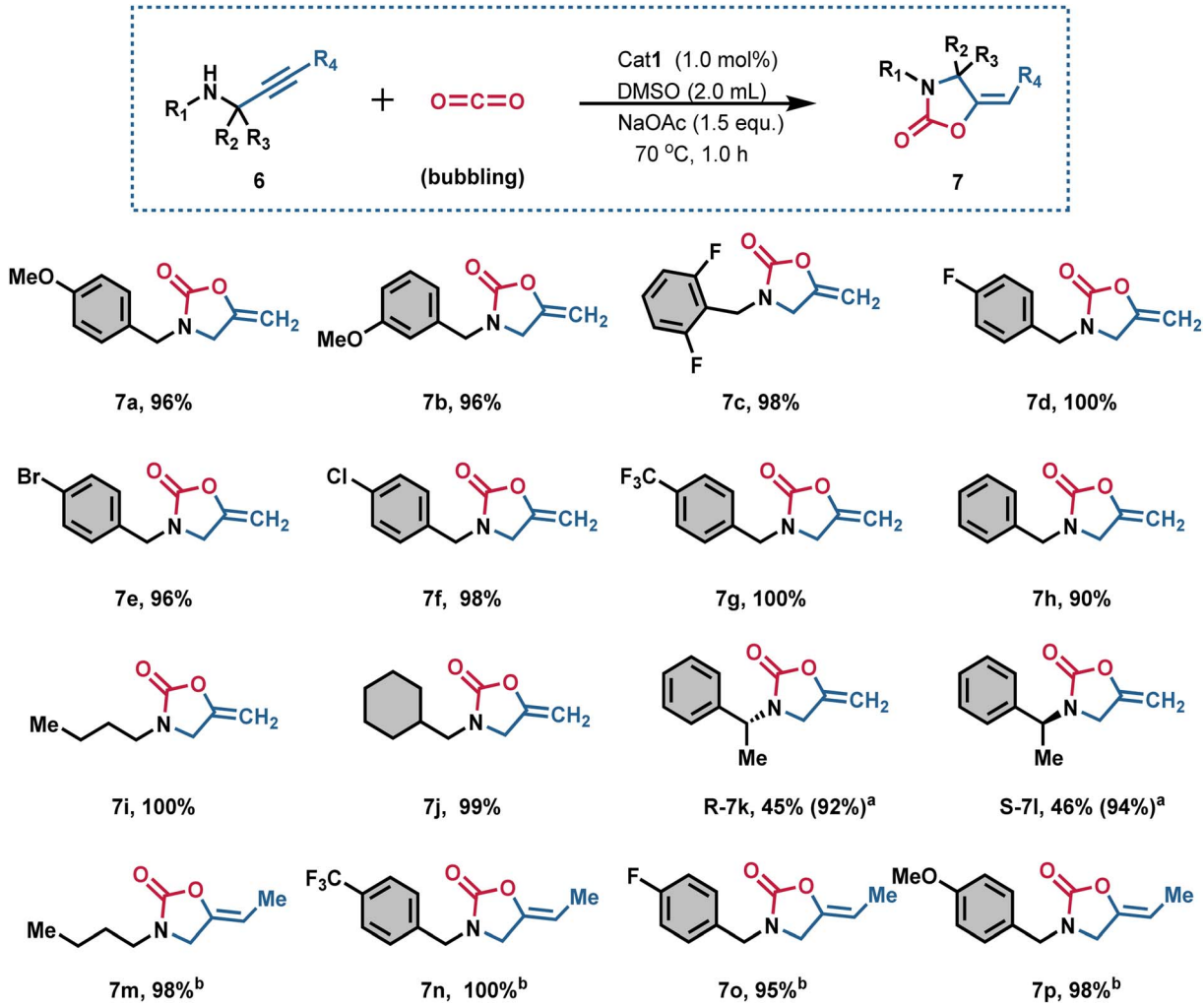

Fig. 4 Scope of the carboxylative cyclization of propargylic amines and CO_2 [simulated flue gas, $V(CO_2) : V(N_2) = 15 : 85$]. Reaction conditions: Cat**1** (1.0 mol%), substrate **6** (0.05 mmol), and NaOAc (1.5 equiv., 0.075 mmol) were added into DMSO (2.0 mL) in the reaction tube, and then stirred at 70 °C for 1.0 h. [a]React for 2.0 h. [b]Cat**1** (1.5 mol%), react for 3.0 h.

negative impact of a Me- group at the terminal alkyne on the reactivity of propargyl amines. Therefore, extending the reaction time to 3.0 h and increasing the amount of catalyst to 1.5 mol% resulted in the formation of target products **7n–7p** with yields ranging from 95% to 100%. Consequently, Cat**1**, containing AcGlu and bis(benzimidazolium) units, can be considered a novel AIO functionalized, efficient Pd catalyst for the carboxylative cyclization of propargylic amines and dilute CO_2. The synthetic utility was further demonstrated by reaction, product conversion, and the synthesis of compound on a gram-scale. Additionally, the gram-scale synthesis was also achieved with good yield. It is worth mentioning that Cat**1**-catalyzed conversion of **6a** and CO_2 into gram-scale **7a** with around 100% yield (Fig. S30†).

Catalyst cycle evaluation

Cat**1** was selected for the recycling reaction to evaluate its stability in the synthesis of 2-oxazolidinone **7a**. Vacuum distillation was utilized to separate the products and Cat**1** after each cycle, while fresh **6a** was introduced into the catalytic system, allowing the solution containing Cat**1** to be recycled for subsequent runs. Then catalyst mixture was recycled for the synthetic reaction and the catalytic activity only decreased by only approximately 10% after 10 cycles by ^{1}H NMR (Fig. S31a and c†). Moreover, the color of the catalytic system remained virtually unchanged throughout runs 1 to 10 (Fig. S31b†), indicating Cat**1** was stabilized during recycling. These results demonstrating that catalyst Cat**1** could be recycled. In contrast, the recyclability of Cat**5** without Ac- units is much lower, whose yield dropped below 85% just after 4 runs (Fig. S32†). These results indicate that the Ac- groups enhance the hydrogen bonding and Lewis acid-Lewis base interactions with $PdCl_4^{2-}$, thereby increasing the stability of the catalytic species during the catalytic process.

The FT-IR and ^{1}H NMR spectra of the Cat**1** were measured before and after recycle (Fig. S33†). The ^{1}H NMR results indicated that the disappearance of bis(benzimidazolium) units after the reaction, while AcGlu units maintained. Furthermore,

changes in the signal peaks corresponding to C=N and C=C in the FT-IR spectrum were observed, while the peaks for C=O, C–O, and C–O–C remained unchanged, further validating our judgments. This would explain the changes in cations and anions would lead to decreased catalytic activity, which further indicated that cations and anions would have a synergistic effect on the catalytic reaction. This would explain the disappearance of the bis(benzimidazolium) units would lead to decreased catalytic activity, which further indicated that among the bis(benzimidazolium), AcGlu, and palladium catalyst species would have a synergistic effect on the catalytic reaction.

Possible mechanism of AIO Cat1-catalyzed carboxylative cyclization

To deepen our understanding of the catalytic mechanism of the AIO Cat**1**-catalyzed carboxylative cyclization reaction, we conducted numerous *quasi-in-situ* NMR and ^{13}C-isotope-labeling experiments. We conducted ^{13}C-isotopic-labeling NMR and FT-IR experiments to verify that the C=O group in product **7a** is derived from CO_2. The results clearly indicate that the peak intensity of the C=O unit in the ^{13}C-labeled **7a** at 155.7 ppm is considerably higher than that of the unlabeled **7a** (Fig. S34a†). Furthermore, from the FT-IR spectra of **7a**, the signal of the C=O unit shifted from 1758 cm^{-1} to 1783 cm^{-1} (Fig. S34b†). These findings provide strong support for our proposed pathway for CO_2 conversion, which entails the initial insertion of CO_2 into the carbonate group of intermediates, leading to the formation of the final 2-oxazolidinones. A broad peak at 2.41 ppm was identified as the NH of substrate **6a** by hydrogen–deuterium exchange ^{1}H NMR experiment in DMSO-d_6 with two drops (70 μL) of D_2O (Fig. S35†).

It is necessary to elucidate the roles of Cat**1** and NaOAc in conjunction with substrate **6a** within the reaction system. Upon the independent addition of Cat**1** and NaOAc, a broad signal at 3.35 ppm appeared while the peak at 2.41 ppm disappeared, suggesting that both components can activate the NH group (Fig. S36†). When Cat**1** and NaOAc were added simultaneously, the shift of the NH peak was very similar to that observed with the addition of only Cat**1** to substrate **6a**, indicating synergistic activation of the NH group by Cat**1** and NaOAc. As illustrated in Fig. S37,† with the progression of the reaction time, the characteristic proton peaks of substrate **6a** (3.08, 3.24, 3.66, and 3.72 ppm) gradually diminished and ultimately vanished, while new characteristic signals for 2-oxazolidinone **7a** (3.74, 4.08, 4.33, and 4.65 ppm) emerged and intensified. These peak changes signify the gradual conversion of substrate **6a** into product **7a**.[13] The dynamics and interactions among Cat**1**, NaOAc, CO_2, and substrate **6a** were further explored using *quasi-in-situ* ^{1}H and ^{13}C

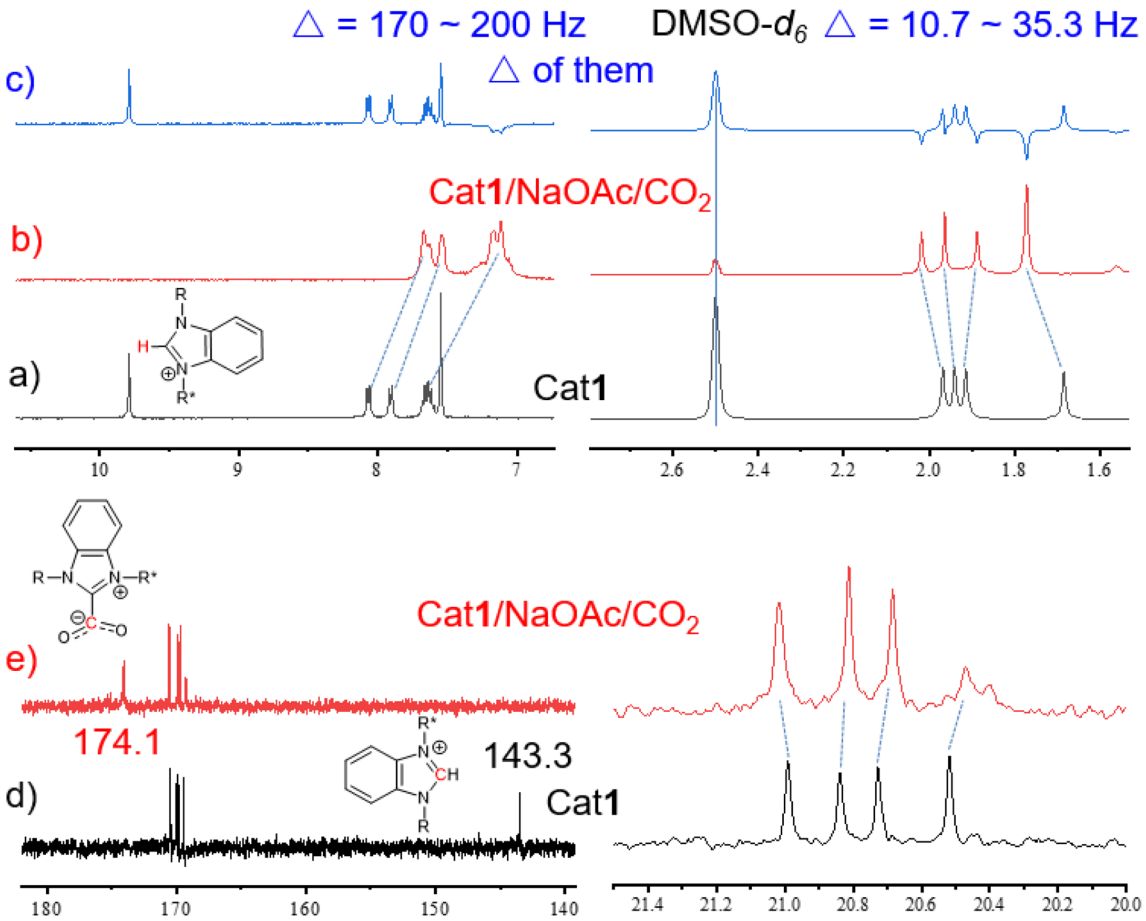

Fig. 5 (a–c) Partially ^{1}H NMR spectra of Cat**1** and Cat**1**/NaOAc/CO_2. (d and e) Partially ^{13}C NMR spectra of Cat**1** and Cat**1**/NaOAc/CO_2.

NMR in DMSO-d_6 (Fig. 5 and S38†). Notably, the proton signals of C_2–H and Ac in Cat**1** shifted upfield significantly by approximately 20 Hz and 5.0 Hz, respectively, after CO_2 was bubbled into DMSO-d_6 (Fig. S38†). This observation underscores the pronounced interactions between Cat**1** and CO_2.

The pK_a values of benzimidazolium salts rang between 21 and 24, positioning them between the ethyl acetate and neutral carbonyl carbon acids such as acetone. This indicates that the least basic NHC is more basic than the most basic phosphine [P(tBu)$_3$, pK_a∼10], suggesting a high proton (C_2–H) affinity.[61–63] Remarkably, the signal at 9.79 ppm assigned to the C_2–H of Cat**1** disappeared upon the introduction of NaOAc, indicating the formation of free NHC even at RT (Fig. 5b). Similarly, the C_2–H peak of imidazolium salt Cat**2** split into a doublet and subsequently disappeared (Fig. S39†), while the proton signal at C_2–Me of Cat**3** remained unchanged (Fig. S40†). The proton signals of Ac groups shifted by 10.7 to 35.3 Hz, and the signals in the benzimidazolium heterocycle broadened and shifted upfield significantly by approximately 170 to 200 Hz (Fig. 5a–c). These results indicate that the weak base NaOAc not only interacts with Cat**1** but also generates free NHC *in-situ*. When CO_2 was bubbled into the mixture of Cat**1**/NaOAc, the proton signals of Ac groups exhibited shifts both upfield and downfield by approximately 10.7 to 35.3 Hz (Fig. 5a–c), indicating the formation of AcGlu-CO_2-philes between CO_2 and Ac groups. Meanwhile, the C_2–C signal at 143.3 ppm disappeared, and a new peak at 174.1 ppm appeared, assigned to the C=O of the *in-situ* formed NHC-CO_2 adducts (Fig. 5d and e).[28] Hence, CO_2 is co-activated in the form of AcGlu-CO_2-philes and NHC-CO_2 adducts, thereby promoting the catalytic process.

As a comparison, when NaOAc was added into the DMSO-d_6 solution of Cat**3** (may be considered as NHO precursor), the ^{1}H NMR signals maintained unchanged (Fig. S40†). This indicates that the alkalinity of NaOAc is insufficient to generate free NHO from Cat**3**, preventing further reaction with CO_2 to form NHO-CO_2 adducts, resulting in lower reaction activity compared to Cat**1**. Herein, the acidity of C_2–H in benzimidazolium salt was found to be superior to that in corresponding Cat**2** and Cat**3**, primarily due to the absence of interfering acidic protons on the ring. It is reasonable to suggest that the formation of NHC-CO_2 adducts from Cat**1** is easier than from Cat**2**, and NHO-CO_2 adducts from Cat**3**.[57] Furthermore, the interactions between Cat**5**, NaOAc, and CO_2 were further investigated *via* ^{1}H NMR. When NaOAc was added to the DMSO-d_6 solution of Cat**5**, the singlet C_2–H peak of the imidazolium ring split into doublet and then disappeared. However, when CO_2 was bubbled into the mixture of Cat**5** and NaOAc, all signals remained unchanged, indicating no interaction between them (Fig. S41†).

Based on these *quasi-in-situ* NMR, ^{13}C-isotope-labeling experiments, and previous studies,[2,11,17] a plausible mechanism has been proposed in Fig. 6. Initially, with the assistance of the base NaOAc, Cat**1** is deprotonated *in-situ* into free NHC (intermediate A). Subsequently, the intermediate A activates CO_2 in the form of NHC-CO_2 adducts (intermediate B). Simultaneously, the AcGlu groups in Cat**1** capture and activate CO_2 in the form of AcGlu-CO_2-philes (intermediate C). In this study, the proton of NH in the propargylic amine is co-deprotonated by NaOAc and Cat**1**, facilitating co-activated CO_2 from intermediates B and C electrophilic attack the amide anion, forming a carbamate intermediate D. The homogeneous $PdCl_4^{2-}$ anion activates the triple bond (C≡C) of terminal alkyne with the assistance of NaOAc, yielding a Pd acetylide intermediate E. Subsequently, the negatively charged oxygen from carbamate intermediate E attacks the Pd acetylide, resulting in intramolecular cyclization (intermediate F). The proton transfer from NaOAc-H$^+$ to the C≡C bond leads to the formation of the

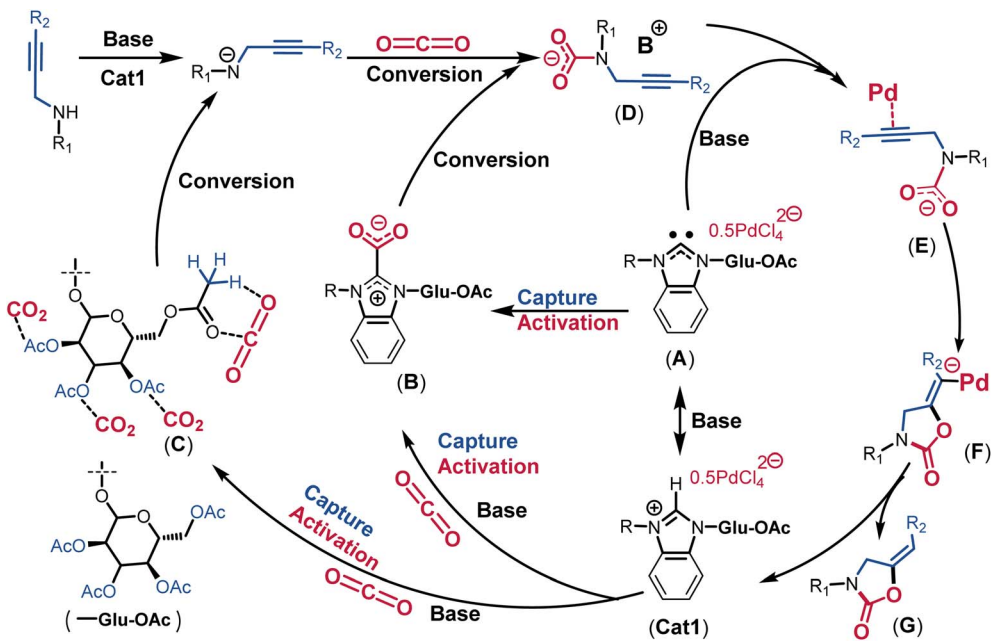

Fig. 6 Proposed mechanism for Cat**1**-catalyzed carboxylative cyclization.

product 2-oxazolidinone G and regenerates Cat**1**. The initial sequestration and activation of CO_2 in the form of NHC-CO_2 adducts and AcGlu-CO_2-philes significantly facilitated the catalytic process. This integrated catalyst demonstrated an interesting multi-dimensional synergistic effect of CO_2 co-sequestration, co-activation, and catalytic transformation in an AIO catalytic system, achieving the highest reported TOF value.

Conclusions

In summary, we have designed a highly efficient Pd catalyst (Cat**1**) through an AIO strategy, functionalized with sugar acetates (AcGlu) and bis(benzimidazolium) units. Cat**1**-catalyzed the cyclization of simulated flue gas and propargylic amine to synthesize 2-oxazolidinone with the highest TOF of 3456 h^{-1}, surpassing all previously reported catalysts. Through a series of *quasi-in situ* NMR and ^{13}C-isotope-labeling experiments, it was observed that the C_2–H in the benzimidazolium heterocycle forms free NHC more readily with the assistance of NaOAc compared to the imidazolium and 2-methylimidazolium heterocycles. In comparison to Cat**5**, which lacks Ac protective groups, the catalytic activity of Cat**1** was significantly enhanced in the cyclization reaction of CO_2 and propargylic amines, demonstrating that the Ac groups enhance CO_2 transformation. The resulting NHC-CO_2 adducts and AcGlu-CO_2-philes served as effective activated CO_2 sources for further conversion. The metal Pd center activated the C≡C bond to generate the Pd acetylide intermediate, leading to the production of a series of 2-oxazolidinones with yields between 90% and 100%. Meanwhile, Cat**1** demonstrated good stability across various temperatures, with catalytic activity decreasing by approximately 10% after 10 cycles. A gram-scale experiment was also conducted to demonstrate the practical scalability of this reaction. This strategy of designing high-performance catalysts with capabilities for activating reaction substrates and stabilizing metal catalytic centers shows great promise for advancing CO_2 conversion technologies. Furthermore, sugar acetates, being low-cost, nontoxic, nonvolatile, biocompatible, and renewable compounds, contribute to making the corresponding CO_2 catalytic reaction process environmentally friendly.

Data availability

The data that support the findings of this study are available in the main text and the ESI.†

Author contributions

Lingfang Kong: investigation, formal analysis, visualization, writing – original draft, writing – review & editing; Zekun Tao: investigation, methodology, formal analysis, writing – original draft; Yunjia Li: investigation, formal analysis; Huiwen Gong: methodology, formal analysis; Yun Bai: methodology, formal analysis, resources, writing – review & editing; Longbin Li: formal analysis, writing – review & editing; Xianjin Zhang: formal analysis, writing – review & editing; Zhonggao Zhou: resources, project administration, supervision, writing – review & editing; Yiwang Chen: resources, project administration, supervision, project administration, writing – review & editing. All the authors discussed the experimental results.

Conflicts of interest

There are no conflicts of interest to declare.

Acknowledgements

This work was financially supported by the National Natural Science Foundation of China Grant Numbers 22261002 (Z. Z.), 22301044 (Y. B.), the Key Project of Jiangxi Provincial Natural Science Foundation 20232ACB203016 (Z. Z.), the Key Laboratory of Jiangxi University for Functional Materials Chemistry Grant Number FMC21702 (Z. Z.), the Innovative Special Fund Project for Graduate Students of Jiangxi Province Grant Number YC2023–S845 (L. K.).

Notes and references

1 F. D. Bobbink, S. Das and P. J. Dyson, *N*-formylation and *N*-methylation of amines using metal-free *N*-heterocyclic carbene catalysts and CO_2 as carbon source, *Nat. Protoc.*, 2017, **12**, 417–428.
2 S.-L. Hou, J. Dong, X.-Y. Zhao, X.-S. Li, F.-Y. Ren, J. Zhao and B. Zhao, Thermocatalytic conversion of CO_2 to valuable products activated by noble-metal-free metal-organic frameworks, *Angew. Chem., Int. Ed.*, 2023, **62**, e202305213.
3 L. Wang, C. Qi, W. Xiong and H. Jiang, Recent advances in fixation of CO_2 into organic carbamates through multicomponent reaction strategies, *Chin. J. Catal.*, 2022, **43**, 1598–1617.
4 J.-H. Ye, T. Ju, H. Huang, L.-L. Liao and D.-G. Yu, Radical carboxylative cyclizations and carboxylations with CO_2, *Acc. Chem. Res.*, 2021, **54**, 2518–2531.
5 R. Cauwenbergh, V. Goyal, R. Maiti, K. Natte and S. Das, Challenges and recent advancements in the transformation of CO_2 into carboxylic acids: straightforward assembly with homogeneous 3d metals, *Chem. Soc. Rev.*, 2022, **51**, 9371–9423.
6 X. Shang, X. Yang, G. Liu, T. Zhang and X. Su, A molecular view of single-atom catalysis toward carbon dioxide conversion, *Chem. Sci.*, 2024, **15**, 4631–4708.
7 G. Ciamician, The Photochemistry of the Future, *Science*, 1912, **36**, 385–394.
8 T. A. Mukhtar and G. D. Wright, Streptogramins, Oxazolidinones, and Other Inhibitors of Bacterial Protein Synthesis, *Chem. Rev.*, 2005, **105**, 529–542.
9 X. Yang, L. Xu, Y. Zhu, S. Zhang, G. Jia and J. Du, Efficient fabrication of oxazolidinones for the carboxylative cyclization with carbon dioxide, *J. CO_2 Util.*, 2023, **74**, 102531.
10 S. Wang and C. Xi, Recent advances in nucleophile-triggered CO_2-incorporated cyclization leading to heterocycles, *Chem. Soc. Rev.*, 2019, **48**, 382–404.

11 L. Li, Y. Lv, H. Sheng, Y. Du, H. Li, Y. Yun, Z. Zhang, H. Yu and M. Zhu, A low-nuclear Ag_4 nanocluster as a customized catalyst for the cyclization of propargylamine with CO_2, *Nat. Commun.*, 2023, **14**, 6989.

12 X. L. Jiang, Y. E. Jiao, S. L. Hou, L. C. Geng, H. Z. Wang and B. Zhao, Green conversion of CO_2 and propargylamines triggered by triply synergistic catalytic effects in metal-organic frameworks, *Angew. Chem., Int. Ed.*, 2021, **60**, 20417–20423.

13 A.-L. Gu, Y.-X. Zhang, Z.-L. Wu, H.-Y. Cui, T.-D. Hu and B. Zhao, Highly efficient conversion of propargylic alcohols and propargylic amines with CO_2 activated by noble-metal-free catalyst Cu_2O@ZIF-8, *Angew. Chem., Int. Ed.*, 2022, **61**, e202114817.

14 F. Inagaki, K. Maeda, K. Nakazawa and C. Mukai, Construction of the Oxazolidinone Framework from Propargylamine and CO_2 in Air at Ambient Temperature: Catalytic Effect of a Gold Complex Featuring an L_2/Z-Type Ligand, *Eur. J. Org Chem.*, 2018, **2018**, 2972–2976.

15 C.-S. Cao, S.-M. Xia, Z.-J. Song, H. Xu, Y. Shi, L.-N. He, P. Cheng and B. Zhao, Highly Efficient Conversion of Propargylic Amines and CO_2 Catalyzed by Noble-Metal-Free $[Zn_{116}]$ Nanocages, *Angew. Chem., Int. Ed.*, 2020, **59**, 8586–8593.

16 X. Xu, Z. Li, H. Huang, X. Jing and C. Duan, A novel copper metal–organic framework catalyst for the highly efficient conversion of CO_2 with propargylic amines, *Inorg. Chem. Front.*, 2022, **9**, 3839–3844.

17 Z.-G. Zhou, P. He, J. Li, J. Zhang, G. Xu, S.-Y. Zhang, X.-X. Deng, Z.-Y. Du, G.-T. Luo, H.-Y. Zhen, Y. Chen and C.-T. He, Integration of CO_2 Capture, Activation, and Conversion with Ternary Acetylglucosyl 2-Methyl-imidazolium Modified Pd Catalyst, *Org. Chem. Front.*, 2023, **10**, 2045–2053.

18 W. Lyu, Y. Liu, J. Zhou, D. Chen, X. Zhao, R. Fang, F. Wang and Y. Li, Modulating the Reaction Configuration by Breaking the Structural Symmetry of Active Sites for Efficient Photocatalytic Reduction of Low-concentration CO_2, *Angew. Chem., Int. Ed.*, 2023, **62**, e202310733.

19 M. Wang, B. Wang, J. Zhang, S. Xi, N. Ling, Z. Mi, Q. Yang, M. Zhang, W. R. Leow, J. Zhang and Y. Lum, Acidic media enables oxygen-tolerant electrosynthesis of multicarbon products from simulated flue gas, *Nat. Commun.*, 2024, **15**, 1218.

20 H. Zhou and X. Lu, Lewis base-CO_2 adducts as organocatalysts for CO_2 transformation, *Sci. China: Chem.*, 2017, **60**, 904–911.

21 I. Sullivan, A. Goryachev, I. A. Digdaya, X. Li, H. A. Atwater, D. A. Vermaas and C. Xiang, Coupling electrochemical CO_2 conversion with CO_2 capture, *Nat. Catal.*, 2021, **4**, 952–958.

22 J. Septavaux, C. Tosi, P. Jame, C. Nervi, R. Gobetto and J. Leclaire, Simultaneous CO_2 capture and metal purification from waste streams using triple-level dynamic combinatorial chemistry, *Nat. Chem.*, 2020, **12**, 202–212.

23 Y. B. Wang, Y. M. Wang, W. Z. Zhang and X. B. Lu, Fast CO_2 sequestration, activation, and catalytic transformation using *N*-heterocyclic olefins, *J. Am. Chem. Soc.*, 2013, **135**, 11996–12003.

24 M. N. Hopkinson, C. Richter, M. Schedler and F. Glorius, An overview of *N*-heterocyclic carbenes, *Nature*, 2014, **510**, 485–496.

25 K. Miharu, N. Bunta, F. Hayato, Y. Kosuke, K. Takuya and T. Mamoru, Single–carbon atom transfer to α,β-unsaturated amides from *N*-heterocyclic carbenes, *Science*, 2023, **379**, 484–488.

26 C.-Y. Wu, W. J. Wolf, Y. Levartovsky, H. A. Bechtel, M. C. Martin, F. D. Toste and E. Gross, High-spatial-resolution mapping of catalytic reactions on single particles, *Nature*, 2017, **541**, 511–515.

27 C. He, D.-H. Si, Y.-B. Huang and R. Cao, A CO_2-masked carbene functionalized covalent organic framework for highly efficient carbon dioxide conversion, *Angew. Chem., Int. Ed.*, 2022, **61**, e202207478.

28 X. Guo, F. Zhang, Z. Yang, L. Gao, R. Wei and G. Xiao, Construction of covalent organic framework functionalized with carbene dual active sites for enhancing CO_2 carboxylation conversion, *Chem. Eng. J.*, 2023, **475**, 146453.

29 L. Wan, M. Pang, J. Le, Z. Xu, H. Zhou, Q. Xu and B. Wang, Oriented intergrowth of the catalyst layer in membrane electrode assembly for alkaline water electrolysis, *Nat. Commun.*, 2022, **13**, 7956.

30 T. Jia, Y.-X. Li, X.-H. Ma, M.-M. Zhang, X.-Y. Dong, J. Ai and S.-Q. Zang, Atomically precise ultrasmall copper cluster for room-temperature highly regioselective dehydrogenative coupling, *Nat. Commun.*, 2023, **14**, 6877.

31 A. Brzeczek-Szafran, K. Erfurt, A. Blacha-Grzechnik, M. Krzywiecki, S. Boncel and A. Chrobok, Carbohydrate Ionic Liquids and Salts as All-in-One Precursors for N-Doped Carbon, *ACS Sustain. Chem. Eng.*, 2019, **7**, 19880–19888.

32 X. Q. Li, K. Chen, R. L. Guo and Z. Wei, Ionic Liquids Functionalized MOFs for Adsorption, *Chem. Rev.*, 2023, **123**, 10432–10467.

33 L. A. Blanchard, D. Hancu, E. J. Beckman and J. F. Brennecke, Green processing using ionic liquids and CO_2, *Nature*, 1999, **399**, 28–29.

34 B. Yoon and G. A. Voth, Elucidating the Molecular Mechanism of CO_2 Capture by Amino Acid Ionic Liquids, *J. Am. Chem. Soc.*, 2023, **145**, 15663–15667.

35 A. Weilhard, S. P. Argent and V. Sans, Efficient carbon dioxide hydrogenation to formic acid with buffering ionic liquids, *Nat. Commun.*, 2021, **12**, 231.

36 Q. Li, F. Yan and J. Texter, Polymerized and Colloidal Ionic Liquids – Syntheses and Applications, *Chem. Rev.*, 2024, **124**, 3813–3931.

37 D. Prodius and A.-V. Mudring, Rare earth metal-containing ionic liquids, *Coord. Chem. Rev.*, 2018, **363**, 1–16.

38 P. Migowski, P. Lozano and J. Dupont, Imidazolium based ionic liquid-phase green catalytic reactions, *Green Chem.*, 2023, **25**, 1237–1260.

39 T. Zhou, C. Gui, L. Sun, Y. Hu, H. Lyu, Z. Wang, Z. Song and G. Yu, Energy Applications of Ionic Liquids: Recent

Developments and Future Prospects, *Chem. Rev.*, 2023, **123**, 12170–12253.

40 X.-B. Hu, Y.-X. Li, K. Huang, S.-L. Ma, H. Yu, Y.-T. Wu and Z.-B. Zhang, Impact of α-D-glucose pentaacetate on the selective separation of CO_2 and SO_2 in supported ionic liquid membranes, *Green Chem.*, 2012, **14**, 1440–1446.

41 P. Raveendran and S. L. Wallen, Sugar acetates as novel, renewable CO_2-philes, *J. Am. Chem. Soc.*, 2002, **124**, 7274–7275.

42 S.-L. Ma, Y.-T. Wu, M. L. Hurrey, S. L. Wallen and C. S. Grant, Sugar Acetates as CO_2-philes: Molecular Interactions and Structure Aspects from Absorption Measurement Using Quartz Crystal Microbalance, *J. Phys. Chem. B*, 2010, **114**, 3809–3817.

43 M. A. Blatchford, P. Raveendran and S. L. Wallen, Spectroscopic Studies of Model Carbonyl Compounds in CO_2: Evidence for Cooperative C–H···O Interactions, *J. Phys. Chem. A*, 2003, **107**, 10311–10323.

44 P. Raveendran and S. L. Wallen, Cooperative C–H···O Hydrogen Bonding in CO_2-Lewis Base Complexes: Implications for Solvation in Supercritical CO_2, *J. Am. Chem. Soc.*, 2002, **124**, 12590–12599.

45 G. Kontos, C. Tsioptsias and I. Tsivintzelis, Cellulose Acetate-Ionic Liquid Blends as Potential Polymers for Efficient CO_2 Separation Membranes, *Polymers*, 2024, **16**, 554.

46 A. Annunziata, A. Amoresano, M. E. Cucciolito, R. Esposito, G. Ferraro, I. Iacobucci, P. Imbimbo, R. Lucignano, M. Melchiorre, M. Monti, C. Scognamiglio, A. Tuzi, D. M. Monti, A. Merlino and F. Ruffo, Pt(II) *versus* Pt(IV) in Carbene Glycoconjugate Antitumor Agents: Minimal Structural Variations and Great Performance Changes, *Inorg. Chem.*, 2020, **59**, 4002–4014.

47 A. Annunziata, M. E. Cucciolito, M. Di Ronza, G. Ferraro, M. Hadiji, A. Merlino, D. Ortiz, R. Scopelliti, F. Fadaei Tirani, P. J. Dyson and F. Ruffo, Ruthenium(II)–Arene Complexes with Glycosylated NHC-Carbene Co-Ligands: Synthesis, Hydrolytic Behavior, and Binding to Biological Molecules, *Organometallics*, 2023, **42**, 952–964.

48 J. Wolfs, R. Nickisch, L. Wanner and M. A. R. Meier, Sustainable One-Pot Cellulose Dissolution and Derivatization *via* a Tandem Reaction in the DMSO/DBU/CO_2 Switchable Solvent System, *J. Am. Chem. Soc.*, 2021, **143**, 18693–18702.

49 T. Hussain Ali, A. Washeel Salman, R. Sabah Abdulhussein, L. Persoons, D. Daelemans, W. Dehaen and L. Van Meervelt, New sugar-incorporated N-heterocyclic carbene precursors and their Ag(I) and Pd(II) complexes: Synthesis, characterization, and cytotoxicity studies, *J. Mol. Liq.*, 2024, **393**, 123618.

50 J. P. Byrne, L. Delgado, F. Paradisi and M. Albrecht, Carbohydrate-Functionalized Triazolylidene Iridium Complexes: Hydrogenation Catalysis in Water with Asymmetric Induction, *ChemCatChem*, 2022, **14**, e202200086.

51 M. Ghosh and S. Khan, N-Heterocyclic Carbenes Capped Metal Nanoparticles: An Overview of Their Catalytic Scope, *Chem. Rev.*, 2023, **13**, 9313–9325.

52 C. He, J. Liang, Y.-H. Zou, J.-D. Yi, Y.-B. Huang and R. Cao, Metal-organic frameworks bonded with metal *N*-heterocyclic carbenes for efficient catalysis, *Natl. Sci. Rev.*, 2022, **9**, nwab157.

53 P. Onnuch, K. Ramagonolla and R. Y. Liu, Aminative Suzuki–Miyaura coupling, *Science*, 2024, **383**, 1019–1024.

54 C.-T. Yue, Q. Xing, P. Sun, Z.-L. Zhao, H. Lv and F.-W. Li, Enhancing stability by trapping palladium inside N-heterocyclic carbene-functionalized hypercrosslinked polymers for heterogeneous C-C bond formations, *Nat. Commun.*, 2021, **12**, 1875.

55 P. García-Domínguez, L. Fehr, G. Rusconi and C. Nevado, Palladium-catalyzed incorporation of atmospheric CO_2: efficient synthesis of functionalized oxazolidinones, *Chem. Sci.*, 2016, **7**, 3914–3918.

56 P. Brunel, J. Monot, C. E. Kefalidis, L. Maron, B. Martin-Vaca and D. Bourissou, Valorization of CO_2: preparation of 2-oxazolidinones by metal–ligand cooperative catalysis with SCS indenediide Pd complexes, *ACS Catal.*, 2017, **7**, 2652–2660.

57 G. Gurau, H. Rodríguez, S. P. Kelley, P. Janiczek, R. S. Kalb and R. D. Rogers, Demonstration of Chemisorption of Carbon Dioxide in 1,3-Dialkylimidazolium Acetate Ionic Liquids, *Angew. Chem., Int. Ed.*, 2011, **50**, 12024–12026.

58 D. Yu and Y. Zhang, Copper- and copper-N-heterocyclic carbene-catalyzed C–H activating carboxylation of terminal alkynes with CO_2 at ambient conditions, *Proc. Natl. Acad. Sci. U.S.A.*, 2010, **107**, 20184–20189.

59 P. Liu, K. Cai, D.-J. Tao and T. Zhao, The mega-merger strategy: M@COF core-shell hybrid materials for facilitating CO_2 capture and conversion to monocyclic and polycyclic carbonates, *Appl. Catal., B*, 2024, **341**, 123317.

60 K. Cai, P. Liu, Z. Chen, P. Chen, F. Liu, T. Zhao and D.-J. Tao, Construction of bifunctional triazine-based imidazolium porous ionomer polymers by a post-crosslinking tactic for efficient CO_2 capture and conversion, *Chem. Eng. J.*, 2023, **451**, 138946.

61 C. Wang, X. Luo, H. Luo, D.-e. Jiang, H. Li and S. Dai, Tuning the Basicity of Ionic Liquids for Equimolar CO_2 Capture, *Angew. Chem., Int. Ed.*, 2011, **50**, 4918–4922.

62 S. Gaillard, C. S. J. Cazin and S. P. Nolan, N-Heterocyclic Carbene Gold(I) and Copper(I) Complexes in C–H Bond Activation, *Acc. Chem. Res.*, 2011, **45**, 778–787.

63 X. li, S. Zeng, A. Wang, G. Li, L. Yuan, K. Peng, C. Jiang, H. Zhang, X. Zhang and S. Zhang, Modulating CO_2 electroreduction to syngas by protic-nonprotic ionic liquid composite electrolytes, *Chem. Eng. Sci.*, 2024, **292**, 119961.